

# 000 001 002 003 004 005 006 007 008 009 010 011 012 013 014 015 016 017 018 019 020 021 022 023 024 025 026 027 028 029 030 031 032 033 034 035 036 037 038 039 040 041 042 043 044 045 046 047 048 049 050 051 052 053 VALUE-STATE GATED ATTENTION FOR MITIGATING EXTREME-TOKEN PHENOMENA IN TRANSFORMERS

Anonymous authors

Paper under double-blind review

## ABSTRACT

Large models based on the Transformer architecture are susceptible to extreme-token phenomena, such as attention sinks and value-state drains. These issues, which degrade model performance, quantization fidelity, and interpretability, arise from a problematic mutual reinforcement mechanism where the model learns an inefficient ‘no-op’ behavior by focusing attention on tokens with near-zero value states. In this paper, we propose Value-State Gated Attention (VGA), a simple, dedicated, and stable architectural mechanism for performing ‘no-op’ attention efficiently by directly breaking this cycle. VGA introduces a learnable, data-dependent gate, computed directly from the value vectors ( $V$ ), to modulate the output. Through a theoretical analysis of the underlying gradients, we show that gating the value-state with a function of itself is more effective at decoupling value and attention score updates than prior methods that gate on input embeddings. This creates a direct regulatory pathway that allows the model to suppress a token’s contribution based on its emergent value representation. Our experiments demonstrate that VGA significantly mitigates the formation of attention sinks and stabilizes value-state norms, leading to improved performance, robust quantization fidelity, and enhanced model interpretability.

## 1 INTRODUCTION

The Transformer architecture has revolutionized artificial intelligence in various domains (Achiam et al., 2023; Dubey et al., 2024; Guo et al., 2025; Dosovitskiy et al., 2020; Brooks et al., 2024). Much of this success stems from the attention mechanism, which allows for efficient and scalable modeling of long-range dependencies. Despite their remarkable success, these models are susceptible to a set of persistent and detrimental emergent behaviors collectively known as **extreme-token phenomena** (Xiao et al., 2023b; Guo et al., 2024; He et al., 2024; Hu et al., 2024). These manifest as a trio of interconnected pathologies: attention sinks (Bondarenko et al., 2023; Guo et al., 2024; Sun et al., 2024; Gu et al., 2024; Barbero et al., 2025; Qiu et al., 2025; Agarwal et al., 2025; Kang et al., 2025), the tendency for certain tokens to receive disproportionately high attention weights regardless of semantic relevance; value-state drains (Guo et al., 2024; Zhou et al., 2024), where the value vectors of these sink tokens exhibit pathologically small norms; and residual-state peaks (Sun et al., 2024; Guo et al., 2024), the abnormal growth of the residual-state norms of the sink token in deeper models.

These interconnected pathologies have profound negative impacts on model performance, quantization fidelity, and interpretability. The pathological growth of residual-state norms induces numerical instability, causing divergence or stagnant learning during training (Zhai et al., 2023). Furthermore, the extreme dynamic range of activations created by these phenomena poses significant challenges for model quantization, often resulting in a substantial accuracy degradation (Bondarenko et al., 2023; Su & Yuan, 2025). Crucially, attention sinks also compromise model interpretability (Bondarenko et al., 2023; Dariset et al., 2023; Wang et al., 2024; Lappe & Giese, 2025), as attention weights no longer reliably indicate semantic importance. The systemic nature of these issues across various Transformer models underscores the need for a fundamental architectural solution.

Recent analyses suggest that these phenomena are not isolated failures, but symptoms of a single underlying pathological feedback loop known as the **mutual reinforcement cycle** (Guo et al., 2024). This cycle arises from the interplay between the optimization dynamics and the competitive nature of the softmax function, which constrains the attention weights to sum to one. The cycle begins when

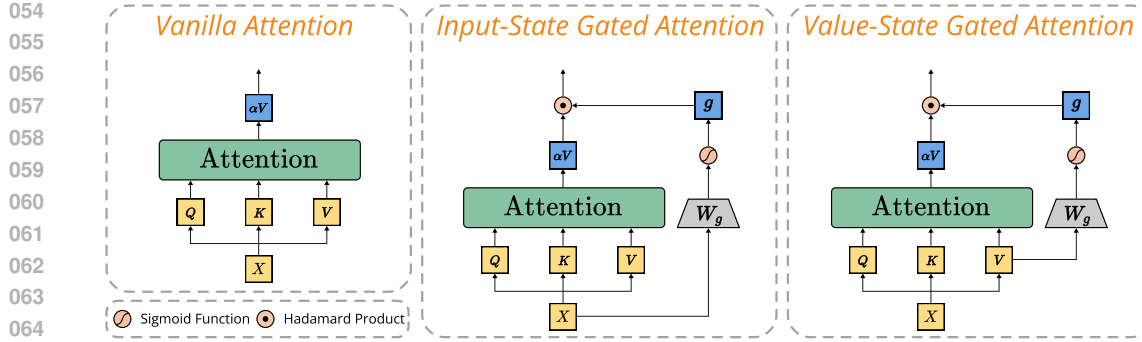


Figure 1: Architecture of Value-State Gated Attention (VGA). Unlike vanilla attention or input-state gated attention, VGA introduces a value-state gating mechanism to modulate the attention output.

an attention head, lacking a relevant context token but forced to distribute its entire attention budget, directs it to a structurally convenient token to perform a ‘no-op’ behavior (Bondarenko et al., 2023; He et al., 2024; Hu et al., 2024), thereby creating an attention sink. To prevent this arbitrarily high attention from corrupting the output, the optimizer reactively minimizes the norm of the sink token’s value vector, leading to a drain of the value state. This drained value state then makes the token an even more attractive target for future ‘no-op’ attention, reinforcing the cycle and locking the model into a stable but pathological equilibrium. The mutual reinforcement cycle is a classic example of an *unstable positive feedback loop* in control theory (Ogata, 2010).

From the analysis of the mutual reinforcement cycle, we observe that the value state is highly indicative of the sink token, which can be leveraged to directly break the mutual reinforcement cycle. Based on this observation, we propose **Value-State Gated Attention (VGA)**, as illustrated in Figure 1, a novel and efficient mechanism that introduces a learnable *negative feedback controller* that stabilizes the optimization dynamics, and enables the model to perform a ‘no-op’ without resorting to attention sinks and value destructions, thus mitigating extreme-token phenomena.

More specifically, we introduce a learnable, value-state dependent gate to modulate the output of the attention head. The core of our approach lies in making the gate’s behavior a reactive function of the value state itself, establishing a direct regulatory pathway that allows the model to suppress a token’s contribution based on its emergent value representation. This design establishes a feedback control system for mitigating extreme-token phenomena. When the optimization process begins to induce a value-state drain, our gate, being directly dependent on this state, learns to close. By closing, the gate severs the gradient flow that drives the value drains. By decoupling high attention from the pressure to suppress value norms, VGA breaks the mutual reinforcement cycle at its core, thereby preventing the formation of extreme-token phenomena.

In this paper, we introduce VGA—a simple dedicated and stable architectural mechanism for efficient performing of ‘no-op’ attention, resolving an inherent optimization conflict in the standard attention, and provide a comprehensive analysis of its theoretical underpinnings. Our empirical validation demonstrates that VGA significantly mitigates the formation of attention sinks and stabilizes value-state norms, leading to improved performance, robust quantization fidelity, and enhanced model interpretability. VGA is intentionally designed to be orthogonal to the attention score computation. By functioning as a lightweight, additive gate on the output, it leaves the capabilities of the attention mechanism intact. This architectural separation makes VGA a general and minimally invasive enhancement, readily applicable to any Transformer-based model.

## 2 RELATED WORK

**Extreme-token phenomena and understanding.** Research on Transformers has identified a set of issues, collectively termed extreme-token phenomena. Initial work identified the phenomenon of attention sinks, where certain tokens attract a disproportionate amount of attention (Xiao et al., 2023b; Darcel et al., 2023; Guo et al., 2024; Gu et al., 2024; Barbero et al., 2025; Qiu et al., 2025; Agarwal et al., 2025; Kang et al., 2025). Subsequent work linked this observation to value-state drains, noting that these same sink tokens consistently have value states with unusually small norms (Guo et al., 2024; Zhou et al., 2024). A mechanistic explanation for this connection was a

108 mutual reinforcement cycle in the training process. This cycle arises when an attention head performs  
 109 a no-op operation (Bondarenko et al., 2023; He et al., 2024; Hu et al., 2024), triggering an irreversible  
 110 loop between high attention weights and the optimizer’s suppression of the corresponding value-state  
 111 norms. Further research in deeper models also documented the emergence of residual-state peaks, an  
 112 abnormal growth in the residual states of sink tokens (Sun et al., 2024; Guo et al., 2024).

113 **Mitigating extreme-token phenomena in post-processing.** Existing methods could be categorized  
 114 into weight-modifying approaches that often involve lightweight fine-tuning (Wang et al., 2024; Chen  
 115 et al., 2024), and state-manipulation approaches that operate intermediate states at inference time  
 116 without altering model weights (Son et al., 2024; Yu et al., 2024; Li et al., 2023). A noteworthy finding  
 117 in Xiao et al. (2024) is the necessity of deliberately reintroducing the “attention sinks” introduced  
 118 from the pre-training phase into downstream tasks to maintain the model’s performance. While  
 119 remedial solutions in the post-processing stage can alleviate problems in the downstream usage of  
 120 pretrained models, a more fundamental approach is to enhance the models’ intrinsic capabilities and  
 121 prevent these issues from arising during the pretraining phase.

122 **Mitigating extreme-token phenomena in pretraining.** Several strategies have been proposed to  
 123 mitigate extreme-token phenomena during pretraining. One line of work introduces special tokens  
 124 that are designed to absorb unneeded attention, such as register tokens (Darcet et al., 2023; Barbero  
 125 et al., 2025; Lappe & Giese, 2025). Another group of researchers modifies the attention mechanism  
 126 itself to prevent or control attention concentration. These proposals include replacing softmax with  
 127 alternative functions (Ramapuram et al., 2024; Gu et al., 2024), adding a clipping function to attention  
 128 scores (Bondarenko et al., 2023), or creating a learnable sink within the mechanism to channel  
 129 attention (Xiao et al., 2023b; Miller, 2023; Agarwal et al., 2025). A third approach uses gating  
 130 to control a token’s contribution. While gating has been widely used in LSTMs (Hochreiter &  
 131 Schmidhuber, 1997) and GRUs (Dey & Salem, 2017), as well as in Transformers(*e.g.*, Yang et al.  
 132 (2024); Gao et al. (2025)), its application to resolve optimization pathologies remains less explored.  
 133 Within this domain, prior approaches (Bondarenko et al., 2023; Qiu et al., 2025) have focused on  
 134 learning the predictive gating function from the input embeddings. While prior methods have focused  
 135 on providing static sinks for extraneous attention or predictive gates based on input features, our  
 136 work is the first to propose a fully reactive, self-regulatory gate that directly addresses the emergent  
 137 optimization dynamics of the value-state.

138 A primary motivation for resolving these phenomena is to improve numerical stability of a model,  
 139 particularly for Post-Training Quantization (PTQ). Extreme-token phenomena create large activation  
 140 outliers, which significantly increases the dynamic range of tensors. This poses a major challenge  
 141 for PTQ methods (Li et al., 2021; Xiao et al., 2023a), as mapping a wide value range to a low-bit  
 142 format can cause substantial precision loss and performance degradation. As noted by Bondarenko  
 143 et al. (2023), models exhibiting extreme-token behaviors are not quantization-friendly. Therefore,  
 144 mitigation strategies applied during pretraining are expected to result in models that are easier to  
 145 quantize. Following this line of reasoning, we adopt a common PTQ methodology (Bondarenko et al.,  
 146 2023) in our experiments to demonstrate that successfully mitigating extreme-token phenomena leads  
 147 to improved post-training quantization results.

### 3 METHOD

149 This section details the theoretical mechanisms of extreme-token phenomena and introduces our  
 150 proposed solution, Value-State Gated Attention. In Section 3.1, we provide a formal gradient-based  
 151 analysis of the mutual reinforcement cycle, first identified by Guo et al. (2024), in the training of  
 152 the standard attention module. We also discuss the pioneering Input-State Gated Attention (IGA)  
 153 approach (Bondarenko et al., 2023; Qiu et al., 2025) for mitigating the extreme-token phenomena.  
 154 Our analysis reveals the limitations of IGA, highlighting that the problem is fundamentally tied  
 155 to the optimization dynamics of the value-state itself, but not the input-state. Building on this  
 156 insight, Section 3.2 details the architecture of VGA, and Section 3.3 provides a theoretical analysis  
 157 demonstrating how its design inherently breaks this cycle by altering the gradient dynamics.

#### 3.1 PRELIMINARIES

158 For clarity, our discussion focuses on the vanilla single-head self-attention, although the principle we  
 159 introduce is readily applicable to more complex variants. The mechanism computes a representation  
 160 for each token by attending to all tokens in the input sequence. Given an input sequence  $X \in \mathbb{R}^{n \times d}$ ,

162 it is projected into Query ( $Q$ ), Key ( $K$ ), and Value ( $V$ ) matrices via learnable weight matrices  
 163  $W_Q, W_K, W_V \in \mathbb{R}^{d \times d}$ , such that  $Q = XW_Q$ ,  $K = XW_K$ , and  $V = XW_V$ . The attention weight  
 164 matrix  $\alpha$  is then computed as:

$$165 \quad \alpha = \text{softmax} \left( \frac{QK^T}{\sqrt{d}} \right). \quad (1)$$

166 The final attention output is computed as  $\text{Attention}(Q, K, V) = \alpha V$ . The matrix  $\alpha \in \mathbb{R}^{n \times n}$  contains  
 167 the attention weights, with each element  $\alpha_{ij}$  representing the weight that query  $i$  assigns to key  $j$ .  
 168 The softmax function ensures that the weights for each query are non-negative and sum to one, *i.e.*,  
 169  $\forall i, \sum_{j=1}^n \alpha_{ij} = 1$ . Consequently, the output for the  $i$ -th token  $z_i$  is a convex combination of all value  
 170 vectors in the sequence:

$$172 \quad z_i = \sum_{j=1}^n \alpha_{ij} V_j. \quad (2)$$

173 This formulation becomes problematic when an attention head needs to perform a ‘no-op’ (*i.e.*,  
 174 contribute minimally to the output). Due to the softmax constraint, the head is forced to distribute  
 175 its attention budget across tokens. If no token is semantically relevant, the head may learn to dump  
 176 its attention onto a single, structurally convenient sink token. Guo et al. (2024) first identified this  
 177 underlying issue as the mutual reinforcement cycle: a pathological feedback dynamic that drives  
 178 the formation of attention sinks and the accompanying suppression of their value states (value-state  
 179 drains). To formalize this process, we analyze the cycle from the perspective of gradient dynamics.

180 To understand the optimizer’s behavior, we examine the gradient of the loss  $L$  with respect to an  
 181 arbitrary value vector  $V_j$ . Applying the chain rule to Equation (2), we obtain:

$$183 \quad \frac{\partial L}{\partial V_j} = \sum_{i=1}^n \frac{\partial z_i}{\partial V_j} \frac{\partial L}{\partial z_i} = \sum_{i=1}^n \alpha_{ij} \frac{\partial L}{\partial z_i}, \quad (3)$$

186 where  $\frac{\partial L}{\partial z_i}$  represents the upstream gradient. This reveals a rigid coupling: the gradient flowing to  $V_j$   
 187 is a direct scaling of the upstream gradients by the attention weights  $\alpha_{ij}$ .

188 The severity of this coupling becomes apparent in the limiting case where a token  $s$  becomes a perfect  
 189 attention sink for a query  $i$ , *i.e.*,  $\alpha_{is} \rightarrow 1$ . The gradient flowing to its value vector  $V_s$  from this query  
 190 approaches the full upstream gradient  $\frac{\partial L}{\partial z_i}$ , while all other value vectors  $V_j$  ( $j \neq s$ ) receive a vanishing  
 191 gradient. To perform a ‘no-op’ and minimize the output’s magnitude despite a large attention weight  
 192  $\alpha_{is}$ , the amplified gradient provides a strong signal to reduce the magnitude of  $V_s$ . This forces the  
 193 optimizer to aggressively push the norm of  $V_s$  towards zero, precipitating a value-state drain. As  
 194 illustrated in Figure 2, this initiates *an unstable positive feedback loop*: high attention amplifies the  
 195 gradient to  $V_s$ , the optimizer suppresses its norm, and the resulting inert value state becomes an even  
 196 safer target for future no-op queries.

197 A prominent prior approach, Input-State Gated Attention (IGA) approach (Bondarenko et al., 2023;  
 198 Qiu et al., 2025) is proposed to address the problem, which introduces a gate to control information  
 199 flow. The gate  $g_j$  is computed from the input embeddings  $X_j$  via a learnable weight matrix  $W_g \in$   
 200  $\mathbb{R}^{d \times 1}$ , followed by a sigmoid activation function  $\sigma$ , as  $g_j = \sigma(X_j W_g)$ , modulating the attention  
 201 output as:

$$202 \quad z_i = \sum_{j=1}^n g_j \alpha_{ij} V_j. \quad (4)$$

204 This architecture introduces a crucial second weighting path. The vanilla attention scores  $\alpha$  continue  
 205 to determine where the model attends, while the new input-state gates  $g$  independently determine  
 206 how much information is received. The model learns to predict from  $X_j$  whether token  $j$  is a ‘no-op’  
 207 candidate and closes the gate  $g_j$ . To analyze its effect on the value-state drains, we examine the  
 208 gradient with respect to  $V_j$ . Since  $g_j$  is a function of  $X_j$ , it is treated as a constant with respect to  $V_j$ :

$$209 \quad \frac{\partial L}{\partial V_j} = \sum_{i=1}^n g_j \alpha_{ij} \frac{\partial L}{\partial z_i}. \quad (5)$$

212 When a token becomes an attention sink where  $\alpha_{is} \rightarrow 1$ , the model would learn to close the  
 213 corresponding gate,  $g_s \rightarrow 0$ , to nullify the contribution of the sink token.

214 However, the fundamental coupling remains. The optimizer still perceives a direct path to nullify the  
 215 output by shrinking  $V$ , as the gate  $g$  is based upon  $X$ , not the emergent dynamics of  $V$ . Hence, the  
 216 gating control is predictive and indirect.

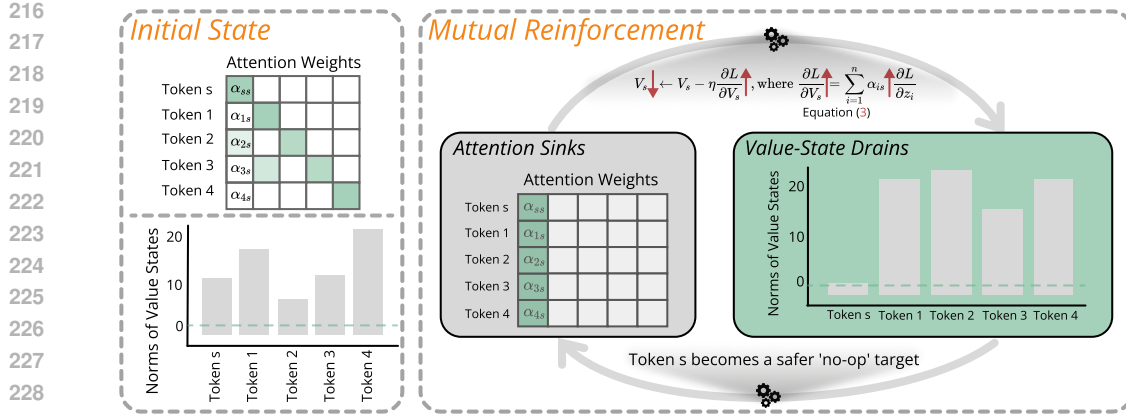


Figure 2: The mutual reinforcement cycle that leads to attention sinks and value-state drains. (Left) Initial state with natural attention weights and moderate value state norms. (Right) The cycle begins when a query allocates high attention to a sink token  $s$ . This amplifies the gradient backpropagated to  $V_s$ , prompting the optimizer to suppress its norm via learning rate  $\eta$ , resulting in a value-state drain. This suppression makes the token an even safer target for future ‘no-op’ queries, locking it into the sink role.

### 3.2 VALUE-STATE GATED ATTENTION

This analysis of IGA reveals the problem’s essence: the instability originates from the optimization pressure applied directly to the value state itself. Therefore, an effective solution cannot be merely predictive; it must be reactive, creating a control directly from the value state. This insight motivates our proposed architecture: Value-State Gated Attention (VGA). As illustrated in Figure 1 (Right), VGA operates as a reactive control system. It introduces a learnable gate computed directly from the value vectors, which modulates each token’s contribution to the attention output. This design endows the model with a direct mechanism to perform a ‘no-op’ by selectively attenuating information flow based on a token’s current value state.

Formally, VGA introduces a gating vector  $g_j$  for each value vector  $V_j$ . This is achieved via a linear projection with a learnable weight matrix  $W_g \in \mathbb{R}^{d \times 1}$ , followed by a sigmoid activation function  $\sigma$ :

$$g_j = \sigma(V_j W_g). \quad (6)$$

These gates are then applied to the output for an individual token  $i$  same as that in Equation (4). A more detailed description of VGA is provided in Appendix B.

The **ONE AND ONLY** critical distinction between IGA and VGA lies in the basis for the gating function: the input-state versus the value-state. Consequently, VGA retains the “second weighting path” advantage of IGA. Moreover, its computational and parameter overhead is identical to IGA, and remains marginal (one projection to low-dimensions and element-wise operations) relative to the total amount of the vanilla model.

### 3.3 HOW VGA BREAKS THE MUTUAL REINFORCEMENT

We now demonstrate how the minimal change of gating basis from input-state to value-state acts as a *learnable negative feedback controller* that stabilizes the optimization dynamics and breaks the mutual reinforcement cycle by dramatically altering the gradient landscape. As shown in Figure 3, VGA decouples attention magnitude from gradient flow through a reactive control mechanism.

270 **Gradient dynamics in VGA.** In VGA, a value vector  $V_j$  influences the output in two ways: it  
 271 provides the semantic content, and it also determines its own transmission strength via the gate  
 272 computation. This necessitates applying the product rule when deriving the gradient of the loss  $L$   
 273 with respect to  $V_j$ . Considering the contribution from a single query  $i$  for clarity, the gradient is:

$$274 \quad \frac{\partial L}{\partial V_j} = \sum_{i=1}^n \alpha_{ij} \frac{\partial(g_j V_j)}{\partial V_j} \frac{\partial L}{\partial z_i}. \quad (7)$$

277 The derivative of the gated value expands into two components corresponding to the two influence  
 278 paths:

$$279 \quad \frac{\partial L}{\partial V_j} = \sum_{i=1}^n \alpha_{ij} \left( \underbrace{g_j I}_{\text{Content Path}} + \underbrace{g_j(1 - g_j) W_g V_j}_{\text{Self-regulatory Path}} \right) \frac{\partial L}{\partial z_i}, \quad (8)$$

283 where the ‘Content Path’ term,  $g_j I$ , reflects the gradient through the vector’s role as content, mod-  
 284 ulated by its gate  $g_j$ . The ‘Self-regulatory Path’ arises from the self-referential design, where  $V_j$   
 285 influences its own gate. This formulation is the key to VGA’s efficacy. We analyze its behavior in the  
 286 critical scenario where a token  $s$  is an attention sink ( $\alpha_{is} \rightarrow 1$ ) and the model has learned to close  
 287 its gate ( $g_s \rightarrow 0$ ). In this limit, both gradient paths are nullified: (1) The ‘Content Path’ term  $g_s I$   
 288 vanishes as  $g_s \rightarrow 0$ ; (2) The ‘Self-regulatory Path’ term also vanishes, as it contains both  $g_s$  and the  
 289 sigmoid derivative factor  $g_s(1 - g_s)$ , which also approaches zero. Consequently, the gradient flowing  
 290 to  $V_s$  is entirely severed:  $\frac{\partial L}{\partial V_s} \rightarrow 0$ , as  $g_s \rightarrow 0$ . This demonstrates that VGA successfully decouples  
 291 the attention weight from the gradient magnitude. Even when attention is maximal, closing the gate  
 292 provides a clean ‘no-op’ mechanism that breaks the link between high attention and the pathological  
 293 gradient amplification, thus dismantling the mutual reinforcement cycle. This analysis demonstrates  
 294 that VGA provides a direct gradient pathway to perform a ‘no-op’ without value-state suppression.  
 295 Our empirical validation in Section 4.1 confirms that the optimizer successfully learns to utilize this  
 296 mechanism, preferring to close the gate rather than pathologically shrinking the value norms.

296 Also note that the term  $g_j(1 - g_j)$  in the ‘Self-regulatory Path’ is maximal when the gate is in its most  
 297 uncertain state ( $g_j = 0.5$ ) and diminishes as the gate becomes confident in its decision (approaching  
 298 0 or 1). This ensures that the self-regulatory feedback is strongest when it is most needed—during  
 299 the transition—and weakest when the gate is already in a stable open or closed state. This property  
 300 prevents runaway feedback loops and is a hallmark of a well-designed, stable control system.

## 302 4 EXPERIMENTS

304 Extensive experiments and comparisons are conducted to demonstrate the advantage of VGA in  
 305 various settings. We begin in Section 4.1 by validating VGA on a specifically designed synthetic task  
 306 as proposed by Guo et al. (2024). Then we evaluate VGA on several language models in Section 4.2,  
 307 including BERT and OPT—following the practice of Bondarenko et al. (2023), as well as GPT-2—a  
 308 seminal autoregressive model whose design became the foundation for numerous subsequent large-  
 309 scale commercial models, and the evidence from which is highly instructive for training large-scale  
 310 commercial LLMs (Allen-Zhu, 2024). Finally, we show the quantization results of BERT and OPT  
 311 models (again, following the practice of Bondarenko et al. (2023)) with VGA in Section 4.3.

### 312 4.1 EMPIRICAL VALIDATION ON THE BIGRAM-BACKCOPY TASK

314 To empirically validate our analysis, we use the Bigram-Backcopy (BB) task from Guo et al. (2024).  
 315 This synthetic task is specifically designed to create a controlled environment where extreme-token  
 316 phenomena are reliably induced. Data generation follows two rules based on token identity: 1) **Bi-**  
 317 **gram task:** For most non-trigger tokens, the next token is generated from a fixed bigram probability  
 318 distribution, similar to a Markov chain. The attention mechanism provides no useful information  
 319 for this task. 2) **Backcopy task:** When predefined trigger tokens (e.g.,  $\text{t}$ ) is encountered, the model  
 320 must ignore the bigram rule and instead copy the token preceding the trigger. This task requires the  
 321 attention mechanism to focus specifically on the token to be copied. We trained two models on this  
 322 task: a vanilla Transformer and one with VGA. The results are presented in Figure 4 and Figure 5.

323 **Attention sinks.** Figure 4(a) shows that the two models exhibit clearly distinct attention patterns. The  
 324 vanilla model (left) exhibits a prototypical attention sink. For all non-trigger query tokens, attention

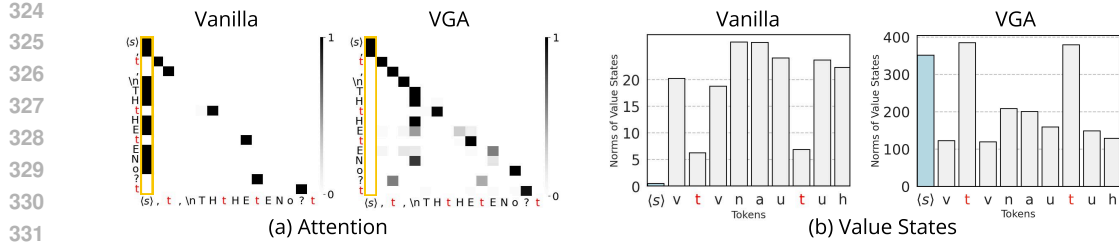


Figure 4: Comparative analysis of a vanilla Transformer (left) and a VGA model (right) on the Bigram-Backcopy (Guo et al., 2024) task. (a) VGA prevents the formation of an attention sink on the  $< s >$  token. (b) Consequently, VGA resolves the corresponding value-state drain, preserving the norm of the sink token’s value vector.

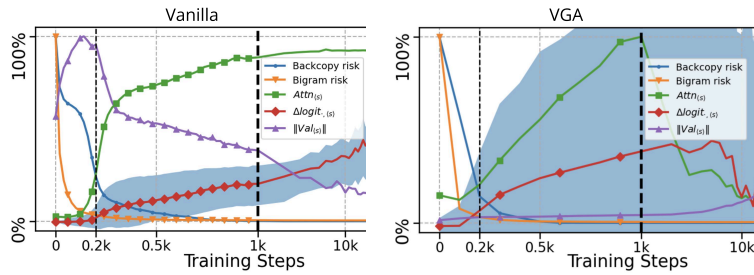


Figure 5: Training dynamics of a vanilla Transformer (left) versus a VGA model (right) on the Bigram-Backcopy task, tracking task performance and sink-token metrics over training steps.

collapses onto the  $< s >$  (start) token, which carries no semantic information for these queries. In contrast, VGA (right) mitigates this behavior. The attention weights are more evenly distributed, and no single token acts as a universal sink, demonstrating that VGA effectively prevents the pathological concentration of attention.

**Value-state drains.** Mitigating attention sinks directly corresponds to the stabilization of value-state norms, as illustrated in Figure 4(b). In the vanilla model (left), the  $< s >$  token suffers from a severe value-state drain, with its norm aggressively reduced toward zero. This reflects the optimizer’s response to the high attention weights, consistent with theoretical analysis. In the VGA model (right), this pathology is absent. The norm of the  $< s >$  token’s value state is maintained at a healthy, non-pathological level comparable to other tokens in the sequence, confirming that our mechanism removes the pressure to destroy value representations.

**Training dynamics.** The evolution of key metrics during training, presented in Figure 5, provides clear evidence that VGA breaks the mutual reinforcement cycle. We track several metrics: (i) Backcopy risk and Bigram risk measure model performance on the two sub-tasks, with lower values being better. (ii)  $Attn_{<s>}$  is the average attention weight directed to the  $< s >$  token from non-trigger queries. (iii)  $\|Val_{<s>}\|$  is the L2 norm of the  $< s >$  token’s value state. (iv)  $\Delta logit_{<s>}$  is calculated by taking the attention logit for the sink key  $< s >$  and subtracting the mean of the logits for all other keys, averaged over non-trigger queries. A higher  $\Delta logit_{<s>}$  indicates a stronger pre-softmax bias toward the sink token. The vanilla model (left) exhibits the cycle’s characteristic signature: as the model learns,  $Attn_{<s>}$  and  $\Delta logit_{<s>}$  steadily increase. Concurrently,  $\|Val_{<s>}\|$  collapses toward zero. This inverse relationship is the hallmark of the pathological feedback loop. The dynamics of the VGA model (right) present a fundamentally different result. While the model learns the task equally well, the pathological signals all remain stable at healthy, non-extreme levels throughout training.

**Enhanced interpretability.** VGA enhances interpretability by using a gate  $g_j$  to disentangle a token’s attention weight from its informational contribution. This provides an explicit signal for a ‘no-op’ operation, where high attention can be paired with a near-zero gate. This resolves a key ambiguity of vanilla attention, where a high attention score can signify either importance or pathology. The results in Figure 4 validate this enhancement by illustrating the vanilla model’s ambiguous state, where high attention on the sink token is paired with the suppression of its value norm. The VGA model exhibits stable attention and value norms, demonstrating its dedicated no-op mechanism prevents the formation of the pathological attention sinks. Consequently, VGA’s attention patterns become a more faithful and reliable indicator of the model’s internal information seeking process.

378 Table 1: Comparison of our proposed VGA against several baselines on BERT (Devlin et al.,  
 379 2019), OPT-125m (Zhang et al., 2022), and GPT-2 (Radford et al., 2019) models. We evaluate task  
 380 performance using Perplexity and model stability by measuring the Max I+O Norm and Avg. kurtosis  
 381 to quantify activation outliers. The best result for each metric is marked in bold. VGA consistently  
 382 delivers top-tier perplexity while suppressing extreme values, demonstrating its dual benefit of  
 383 boosting performance and improving model stability.

Model	Method	Perplexity ( $\downarrow$ )	Max I+O Norm ( $\downarrow$ )	Avg. kurtosis ( $\downarrow$ )
BERT	Vanilla	$4.52 \pm 0.03$	$812.39 \pm 141.62$	$2987.23 \pm 313.21$
	Register Tokens	$4.53 \pm 0.01$	$1205.91 \pm 223.14$	$7812.73 \pm 1281.12$
	Learnable Sink	$4.53 \pm 0.02$	$41.65 \pm 7.83$	$225.88 \pm 41.81$
	IGA	$4.53 \pm 0.01$	$38.71 \pm 10.19$	$90.65 \pm 5.78$
	VGA	$4.52 \pm 0.00$	$33.19 \pm 6.75$	$84.55 \pm 2.84$
OPT	Vanilla	$15.95 \pm 0.03$	$1.01 \pm 0.04$	$2177 \pm 274$
	Register Tokens	$15.85 \pm 0.04$	$0.75 \pm 0.03$	$8322.68 \pm 1197.74$
	Learnable Sink	$15.92 \pm 0.01$	$0.77 \pm 0.03$	$22.23 \pm 6.77$
	IGA	$15.65 \pm 0.01$	$0.50 \pm 0.02$	$102 \pm 1.32$
	VGA	$15.49 \pm 0.00$	$0.45 \pm 0.03$	$34.77 \pm 4.65$
GPT-2	Vanilla	$17.03 \pm 0.00$	$256.84 \pm 18.77$	$13412.71 \pm 3.528.30$
	Register Tokens	$16.26 \pm 0.01$	$73.81 \pm 5.86$	$4871.96 \pm 803.12$
	Learnable Sink	$16.51 \pm 0.00$	$14.50 \pm 2.27$	$71.08 \pm 6.32$
	IGA	$16.62 \pm 0.01$	$17.68 \pm 4.41$	$33.51 \pm 5.29$
	VGA	$16.52 \pm 0.01$	$12.37 \pm 1.28$	$31.27 \pm 6.71$

396 Note that the solution proposed by Guo et al. (2024) involves replacing softmax with ReLU, which is  
 397 a fundamental alteration to the attention mechanism. Although softmax contributes to the mutual  
 398 reinforcement cycle, it remains central to the model’s ability to allocate its finite attention budget.  
 399 Removing it, as suggested by the use of ReLU, may have unforeseen consequences on model  
 400 expressivity and behavior. VGA, in contrast, is a lightweight, additive component. It preserves  
 401 the well-understood properties of the standard softmax-based attention mechanism while surgically  
 402 correcting a specific failure mode. This makes VGA a more practical and readily adoptable solution.  
 403

## 4.2 RESULTS ON REPRESENTATIVE LANGUAGE MODELS

406 We evaluate our proposed VGA method on several representative transformer-based language models  
 407 to assess its impact on model performance and activation stability. Experiments follow the framework  
 408 of Bondarenko et al. (2023) to show that VGA effectively mitigates the extreme-token phenomenon.

409 **Models and Datasets.** Our evaluation includes three representative language models: BERT (Devlin  
 410 et al., 2019), OPT-125m (Zhang et al., 2022), and GPT-2 (Radford et al., 2019). Following previous  
 411 work (Bondarenko et al., 2023), we evaluate BERT and OPT-125m on a combined dataset of  
 412 BookCorpus (Zhu et al., 2015) and English Wikipedia (Guo et al., 2020). Our GPT-2 implementation  
 413 follows Karpathy (2022) and incorporates Rotary Position Embeddings (RoPE) (Su et al., 2024),  
 414 a widely adopted technique in modern Transformer architectures. We train the 124M parameter  
 415 variant<sup>1</sup> of GPT-2 on the OpenWebText (Gao et al., 2020) dataset.

416 **Evaluation metrics.** We use Perplexity (Jelinek et al., 1977) to evaluate the overall language  
 417 modeling performance, where lower values indicate a better predictive capability. To measure  
 418 activation stability, we adopt two metrics as in Bondarenko et al. (2023). We use the maximum  
 419 input and output norm (Max I+O Norm) to quantify the magnitude of the most extreme outliers and  
 420 the average kurtosis (Avg. kurtosis) to measure the heavy-tailedness of the activation distributions.  
 421 Lower values for both metrics indicate better-behaved distributions, which is crucial for effective  
 422 quantization (Chmiel et al., 2020; Bondarenko et al., 2021).

423 **Baselines.** Our chosen baselines are representative of the primary competing paradigms for mitigating  
 424 extreme-token phenomena, as categorized in our review of related work, allowing for a direct  
 425 comparison of these distinct approaches. The vanilla softmax attention mechanism serves as our  
 426 primary benchmark (Vaswani et al., 2017). We also evaluate against Register Tokens (Darcet et al.,  
 427 2023; Lappe & Giese, 2025), a method that prepends a set of learnable non-semantic tokens as  
 428 alternative targets for attention heads. Furthermore, we compare with Learnable Sink (Xiao et al.,  
 429 2023b; Agarwal et al., 2025), which introduces a dedicated token to absorb superfluous attention  
 430 scores and stabilize attention patterns—a method that serves as a representative for the broader class

431 <sup>1</sup>The training of GPT-2 (124M) requires  $8 \times$  A100 40GB for about 5 days. Training larger variants of GPT-2  
 432 required resources beyond the scope of this study.

432 Table 2: Evaluation of post-training quantization on BERT and OPT.  $\Delta$ Perplexity denotes the  
 433 perplexity increase relative to the FP32 baseline presented in Table 1.

Model	Method	INT8 Perplexity ( $\downarrow$ )	$\Delta$ Perplexity (vs. FP32) ( $\downarrow$ )	Max I+O Norm ( $\downarrow$ )	Avg. kurtosis ( $\downarrow$ )
BERT	Vanilla	617.32 $\pm$ 191.20	+612.80	486.19 $\pm$ 227.62	2508.21 $\pm$ 1394.71
	Register Tokens	913.67 $\pm$ 839.10	+909.14	415.27 $\pm$ 218.05	7,284.18 $\pm$ 3,365.82
	Learnable Sink	4.79 $\pm$ 0.03	+0.26	42.82 $\pm$ 2.69	153.47 $\pm$ 38.97
	IGA	4.67 $\pm$ 0.01	+0.15	45.06 $\pm$ 1.50	91.27 $\pm$ 2.88
	VGA	<b>4.64<math>\pm</math>0.01</b>	<b>+0.12</b>	<b>37.1<math>\pm</math>2.37</b>	<b>78.32<math>\pm</math>1.82</b>
OPT	Vanilla	43.78 $\pm$ 6.81	+27.83	657.77 $\pm$ 240.89	6548.18 $\pm$ 1567.07
	Register Tokens	123.81 $\pm$ 91.77	+107.96	835.33 $\pm$ 274.83	6646.24 $\pm$ 3735.05
	Learnable Sink	17.31 $\pm$ 0.01	+1.39	114.45 $\pm$ 4.05	26.35 $\pm$ 4.26
	IGA	16.77 $\pm$ 0.01	+1.12	102.15 $\pm$ 3.81	95.48 $\pm$ 6.12
	VGA	<b>16.42<math>\pm</math>0.01</b>	<b>+0.93</b>	<b>100.01<math>\pm</math>3.44</b>	<b>18.34<math>\pm</math>1.65</b>

438 of strategies on providing an escape from the softmax constraint (Ramapuram et al., 2024; Gu et al.,  
 439 2024; Bondarenko et al., 2023). Finally, we consider IGA (Bondarenko et al., 2023), representing  
 440 prior methods that learn the gating function from the input embeddings.

441 **Results analysis.** The results in Table 1 demonstrate VGA’s dual benefit of improving performance  
 442 while decisively enhancing model stability. Its consistent superiority in reducing Max I+O Norm and  
 443 Avg. kurtosis across all models indicates a fundamental taming of activation outliers. We observe that  
 444 other baselines have inherent design limitations. Register Tokens merely provide an alternative sink  
 445 and can even exacerbate Avg. kurtosis. While Learnable Sink improves stability, its sink mechanism is  
 446 based on a fixed embedding learned during training, making it incapable of adapting to specific input  
 447 contexts. In contrast, VGA uses dynamic, data-dependent gating. Similarly, IGA’s predictive gating  
 448 on input embeddings is shown to be less effective at decoupling value-attention updates compared to  
 449 VGA’s reactive mechanism, which operates directly on the emergent value-state. Consequently, VGA  
 450 provides a more structural solution, one that systemically moderates the entire activation distribution.  
 451 This makes VGA a robust approach to improving reliability without compromising performance.

### 452 4.3 POST TRAINING QUANTIZATION RESULTS

453 We evaluated our method using an 8-bit post-training quantization (PTQ) scheme, following the  
 454 settings in Bondarenko et al. (2023). As shown in Table 2, the baseline Vanilla models exhibit a large  
 455 perplexity increase after quantization, corresponding to their high Max I+O Norm and Avg. kurtosis.  
 456 Notably, Register Tokens results in even greater performance loss. This suggests that simply providing  
 457 a dedicated sink may concentrate pathological dynamics and exacerbate outlier issues, as evidenced  
 458 by its extremely high kurtosis. In contrast, all mitigation methods improve quantization robustness,  
 459 with VGA consistently performing best. On both BERT and OPT, VGA achieves the smallest  
 460 perplexity increase while also recording the lowest Max I+O Norm and lowest Avg. kurtosis. These  
 461 results indicate that by addressing the formation of extreme-token phenomena at its source, VGA  
 462 produces a model with an inherently more quantization-friendly activation distribution. Encouraged  
 463 by these PTQ results, we plan to incorporate VGA in low-bit pretraining in future work.

## 464 5 CONCLUSION

465 In this work, we introduced Value-State Gated Attention (VGA) as a novel and efficient mechanism  
 466 for mitigating extreme-token phenomena. By computing a learnable gate directly from the value  
 467 states, VGA creates a self-regulatory mechanism that enables a ‘no-op’ operation, architecturally  
 468 decoupling high attention weights from the destructive pressure on value norms. Through both  
 469 gradient-based theoretical analysis and empirical validation on synthetic tasks and standard models,  
 470 we demonstrated that VGA effectively mitigates extreme-token phenomena. This directly translates  
 471 to significant improvements in activation stability and post-training quantization fidelity, often while  
 472 maintaining or enhancing model perplexity.

473 As a general design for Transformers, VGA has high potential to be effective in any Transformer-  
 474 based models, from language models, to vision and multi-modal models, especially when they  
 475 are scaled up to even larger models, where extreme-token phenomena are even more pronounced.  
 476 However, such large-scale experiments demand a level of computational resources that places them  
 477 beyond the scope of the present study. We therefore hope that our work will encourage research  
 478 groups with access to these resources to investigate VGA’s performance in such settings—with only  
 479 a few lines of code modification. We are optimistic that it will prove to be an impactful component  
 480 for the next generation of large-scale models across various domains.

486 REFERENCES  
487

488 Josh Achiam, Steven Adler, Sandhini Agarwal, Lama Ahmad, Ilge Akkaya, Florencia Leoni Aleman,  
489 Diogo Almeida, Janko Altenschmidt, Sam Altman, Shyamal Anadkat, et al. GPT-4 technical report.  
490 *arXiv preprint arXiv:2303.08774*, 2023.

491 Sandhini Agarwal, Lama Ahmad, Jason Ai, Sam Altman, Andy Applebaum, Edwin Arbus, Rahul K  
492 Arora, Yu Bai, Bowen Baker, Haiming Bao, et al. gpt-oss-120b & gpt-oss-20b Model Card. *arXiv*  
493 *preprint arXiv:2508.10925*, 2025.

494 Zeyuan Allen-Zhu. ICML 2024 Tutorial: Physics of Language Models, July 2024. Project page:  
495 <https://physics.allen-zhu.com/>.

496 Federico Barbero, Alvaro Arroyo, Xiangming Gu, Christos Perivolaropoulos, Michael Bronstein,  
497 Petar Veličković, and Razvan Pascanu. Why do LLMs attend to the first token? *arXiv preprint*  
498 *arXiv:2504.02732*, 2025.

499 Yelysei Bondarenko, Markus Nagel, and Tijmen Blankevoort. Understanding and overcoming the  
500 challenges of efficient transformer quantization. *arXiv preprint arXiv:2109.12948*, 2021.

501 Yelysei Bondarenko, Markus Nagel, and Tijmen Blankevoort. Quantizable transformers: Removing  
502 outliers by helping attention heads do nothing. *Advances in Neural Information Processing Systems*,  
503 2023.

504 Tim Brooks, Bill Peebles, Connor Holmes, Will DePue, Yufei Guo, Li Jing, David Schnurr, Joe  
505 Taylor, Troy Luhman, Eric Luhman, et al. Video generation models as world simulators. *OpenAI*  
506 *Blog*, 2024.

507 Jiun-Man Chen, Yu-Hsuan Chao, Yu-Jie Wang, Ming-Der Shieh, Chih-Chung Hsu, and Wei-Fen Lin.  
508 Quanttune: Optimizing model quantization with adaptive outlier-driven fine tuning. *arXiv preprint*  
509 *arXiv:2403.06497*, 2024.

510 Brian Chmiel, Ron Banner, Gil Shomron, Yury Nahshan, Alex Bronstein, Uri Weiser, et al. Robust  
511 quantization: One model to rule them all. In *Advances in neural information processing systems*,  
512 2020.

513 Timothée Darcet, Maxime Oquab, Julien Mairal, and Piotr Bojanowski. Vision transformers need  
514 registers. In *International Conference on Learning Representations*, 2023.

515 Jacob Devlin, Ming-Wei Chang, Kenton Lee, and Kristina Toutanova. Bert: Pre-training of deep  
516 bidirectional transformers for language understanding. In *Proceedings of the 2019 conference of*  
517 *the North American chapter of the association for computational linguistics: human language*  
518 *technologies, volume 1 (long and short papers)*, 2019.

519 Rahul Dey and Fathi M Salem. Gate-variants of gated recurrent unit (gru) neural networks. In *2017*  
520 *IEEE 60th international midwest symposium on circuits and systems (MWSCAS)*, 2017.

521 Alexey Dosovitskiy, Lucas Beyer, Alexander Kolesnikov, Dirk Weissenborn, Xiaohua Zhai, Thomas  
522 Unterthiner, Mostafa Dehghani, Matthias Minderer, Georg Heigold, Sylvain Gelly, et al. An image  
523 is worth 16x16 words: Transformers for image recognition at scale. In *International Conference*  
524 *on Learning Representations*, 2020.

525 Abhimanyu Dubey, Abhinav Jauhri, Abhinav Pandey, Abhishek Kadian, Ahmad Al-Dahle, Aiesha  
526 Letman, Akhil Mathur, Alan Schelten, Amy Yang, Angela Fan, et al. The llama 3 herd of models.  
527 *arXiv e-prints:2407.21783*, 2024.

528 Leo Gao, Stella Biderman, Sid Black, Laurence Golding, Travis Hoppe, Charles Foster, Jason Phang,  
529 Horace He, Anish Thite, Noa Nabeshima, Shawn Presser, and Connor Leahy. The Pile: An 800gb  
530 dataset of diverse text for language modeling. *arXiv preprint arXiv:2101.00027*, 2020.

531 Shouwei Gao, Yu Qin, Ruixin Zhu, Zirui Zhao, Hao Zhou, and Zihao Zhu. Sgsaformer: Spike gated  
532 self-attention transformer and temporal attention. *Electronics*, 14(1), 2025. ISSN 2079-9292. doi:  
533 10.3390/electronics14010043. URL <https://www.mdpi.com/2079-9292/14/1/43>.

540 Xiangming Gu, Tianyu Pang, Chao Du, Qian Liu, Fengzhuo Zhang, Cunxiao Du, Ye Wang, and  
 541 Min Lin. When attention sink emerges in language models: An empirical view. In *International*  
 542 *Conference on Learning Representations*, 2024.

543

544 Daya Guo, Dejian Yang, Haowei Zhang, Junxiao Song, Ruoyu Zhang, Runxin Xu, Qihao Zhu,  
 545 Shirong Ma, Peiyi Wang, Xiao Bi, et al. Deepseek-r1: Incentivizing reasoning capability in llms  
 546 via reinforcement learning. *arXiv preprint arXiv:2501.12948*, 2025.

547 Mandy Guo, Zihang Dai, Denny Vrandečić, and Rami Al-Rfou. Wiki-40b: Multilingual language  
 548 model dataset. In *Proceedings of the Twelfth Language Resources and Evaluation Conference*,  
 549 2020.

550

551 Tianyu Guo, Druv Pai, Yu Bai, Jiantao Jiao, Michael I Jordan, and Song Mei. Active-dormant  
 552 attention heads: Mechanistically demystifying extreme-token phenomena in llms. *arXiv preprint*  
 553 *arXiv:2410.13835*, 2024.

554

555 Bobby He, Lorenzo Noci, Daniele Paliotta, Imanol Schlag, and Thomas Hofmann. Understanding and  
 556 minimising outlier features in transformer training. *Advances in Neural Information Processing*  
 557 *Systems*, 2024.

558

559 Sepp Hochreiter and Jürgen Schmidhuber. Long short-term memory. *Neural computation*, 1997.

560

561 Jerry Yao-Chieh Hu, Pei-Hsuan Chang, Haozheng Luo, Hong-Yu Chen, Weijian Li, Wei-Po Wang,  
 562 and Han Liu. Outlier-efficient hopfield layers for large transformer-based models. In *International*  
 563 *Conference on Machine Learning*, 2024.

564

565 Fred Jelinek, Robert L Mercer, Lalit R Bahl, and James K Baker. Perplexity—a measure of the  
 566 difficulty of speech recognition tasks. *The Journal of the Acoustical Society of America*, 62(S1):  
 567 S63–S63, 1977.

568

569 Seil Kang, Jinyeong Kim, Junhyeok Kim, and Seong Jae Hwang. See what you are told: Visual atten-  
 570 tion sink in large multimodal models. In *International Conference on Learning Representations*,  
 571 2025.

572

573 Andrej Karpathy. NanoGPT. <https://github.com/karpathy/nanoGPT>, 2022.

574

575 Alexander Lappe and Martin A Giese. Register and CLS tokens yield a decoupling of local and  
 576 global features in large ViTs. *arXiv preprint arXiv:2505.05892*, 2025.

577

578 Kenneth Li, Oam Patel, Fernanda Viégas, Hanspeter Pfister, and Martin Wattenberg. Inference-time  
 579 intervention: Eliciting truthful answers from a language model. *Advances in Neural Information*  
 580 *Processing Systems*, 2023.

581

582 Yuhang Li, Ruihao Gong, Xu Tan, Yang Yang, Peng Hu, Qi Zhang, Fengwei Yu, Wei Wang, and Shi  
 583 Gu. Brecq: Pushing the limit of post-training quantization by block reconstruction. *arXiv preprint*  
 584 *arXiv:2102.05426*, 2021.

585

586 Evan Miller. Attention is off by one, 2023. URL <https://www.evanmiller.org/attention-is-off-by-one.html>.

587

588 Katsuhiko Ogata. *Modern Control Engineering*. Prentice Hall, 5th edition, 2010.

589

590 Zihan Qiu, Zekun Wang, Bo Zheng, Zeyu Huang, Kaiyue Wen, Songlin Yang, Rui Men, Le Yu, Fei  
 591 Huang, Suozhi Huang, et al. Gated Attention for Large Language Models: Non-linearity, Sparsity,  
 592 and Attention-Sink-Free. *arXiv preprint arXiv:2505.06708*, 2025.

593

594 Alec Radford, Jeffrey Wu, Rewon Child, David Luan, Dario Amodei, Ilya Sutskever, et al. Language  
 595 models are unsupervised multitask learners. *OpenAI blog*, 1(8):9, 2019.

596

597 Jason Ramapuram, Federico Danieli, Eeshan Dhekane, Floris Weers, Dan Busbridge, Pierre Ablin,  
 598 Tatiana Likhomanenko, Jagrit Digani, Zijin Gu, Amitis Shidani, et al. Theory, analysis, and best  
 599 practices for sigmoid self-attention. *arXiv preprint arXiv:2409.04431*, 2024.

594 Seungwoo Son, Wonpyo Park, Woohyun Han, Kyuyeun Kim, and Jaeho Lee. Prefixing attention  
 595 sinks can mitigate activation outliers for large language model quantization. In *Proceedings of the*  
 596 *2024 Conference on Empirical Methods in Natural Language Processing*, 2024.

597

598 Jianlin Su, Murtadha Ahmed, Yu Lu, Shengfeng Pan, Wen Bo, and Yunfeng Liu. Roformer: Enhanced  
 599 transformer with rotary position embedding. *Neurocomput.*, 568(C), February 2024. ISSN 0925-  
 600 2312. doi: 10.1016/j.neucom.2023.127063. URL <https://doi.org/10.1016/j.neucom.2023.127063>.

601

602 Zunhai Su and Kehong Yuan. KVSink: Understanding and Enhancing the Preservation of Attention  
 603 Sinks in KV Cache Quantization for LLMs. In *Second Conference on Language Modeling*, 2025.

604

605 Mingjie Sun, Xinlei Chen, J Zico Kolter, and Zhuang Liu. Massive activations in large language  
 606 models. *arXiv preprint arXiv:2402.17762*, 2024.

607

608 Ashish Vaswani, Noam Shazeer, Niki Parmar, Jakob Uszkoreit, Llion Jones, Aidan N Gomez, Łukasz  
 609 Kaiser, and Illia Polosukhin. Attention is all you need. *Advances in neural information processing*  
 610 *systems*, 2017.

611 Haoqi Wang, Tong Zhang, and Mathieu Salzmann. Sinder: Repairing the singular defects of dinov2.  
 612 In *European Conference on Computer Vision*, 2024.

613

614 Guangxuan Xiao, Ji Lin, Mickael Seznec, Hao Wu, Julien Demouth, and Song Han. Smoothquant:  
 615 Accurate and efficient post-training quantization for large language models. In *International*  
 616 *conference on machine learning*, pp. 38087–38099. PMLR, 2023a.

617

618 Guangxuan Xiao, Yuandong Tian, Beidi Chen, Song Han, and Mike Lewis. Efficient streaming  
 619 language models with attention sinks. In *International Conference on Learning Representations*,  
 620 2023b.

621

622 Guangxuan Xiao, Yuandong Li, Hao Feng, Zichang Zhang, Shangwen Chen, Yu Wang, and Song  
 623 Han. Efficient streaming language models with attention sinks. In *The Twelfth International*  
 624 *Conference on Learning Representations*, 2024.

625

626 Songlin Yang, Huixin Yang, Xinyu Chen, Jiaqi Chen, Jian Qin, Zihan Dai, Jia Tang, Shiliang Jin,  
 627 Xinyu Chen, Min Sun, Jian Lu, Jian Peng, Ming Ma, Xiaoyun Zhang, and Guoliang Wu. Gated  
 628 linear attention transformers with hardware-efficient training. In *ICML '24: Proceedings of the*  
 629 *41st International Conference on Machine Learning*, pp. 41001–41018. PMLR, 2024. doi: 10.  
 630 5555/3692070.3694403. URL <https://proceedings.mlr.press/v235/yang24ab.html>.

631

632 Zhongzhi Yu, Zheng Wang, Yonggan Fu, Huihong Shi, Khalid Shaikh, and Yingyan Lin. Unveiling  
 633 and harnessing hidden attention sinks: enhancing large language models without training through  
 634 attention calibration. In *International Conference on Machine Learning*, 2024.

635

636 Shuangfei Zhai, Tatiana Likhomanenko, Etaı Littwin, Dan Busbridge, Jason Ramapuram, Yizhe  
 637 Zhang, Jiatao Gu, and Joshua M Susskind. Stabilizing transformer training by preventing attention  
 638 entropy collapse. In *International Conference on Machine Learning*, 2023.

639

640 Susan Zhang, Stephen Roller, Naman Goyal, Mikel Artetxe, Moya Chen, Shuhui Chen, Christopher  
 641 Dewan, Mona Diab, Xian Li, Xi Victoria Lin, et al. Opt: Open pre-trained transformer language  
 642 models. *arXiv preprint arXiv:2205.01068*, 2022.

643

644 Zhanhao Zhou, Tianyi Wu, Zhiyun Jiang, and Zhenzhong Lan. Value residual learning for alleviating  
 645 attention concentration in transformers. *arXiv preprint arXiv:2410.17897*, 2024.

646

647 Yukun Zhu, Ryan Kiros, Rich Zemel, Ruslan Salakhutdinov, Raquel Urtasun, Antonio Torralba, and  
 648 Sanja Fidler. Aligning books and movies: Towards story-like visual explanations by watching  
 649 movies and reading books. In *Proceedings of the IEEE international conference on computer*  
 650 *vision*, 2015.

648 A GRADIENT DERIVATION FOR VALUE-STATE GATED ATTENTION (VGA)  
649650 Let  $V_j \in \mathbb{R}^{1 \times d}$  be the row vector value for token  $j$ ,  $\alpha_{ij}$  the attention weight of query  $i$  to token  $j$ ,  
651 and  $W_g \in \mathbb{R}^{d \times 1}$  the gate projection weight. The gate scalar is computed as:  
652

653 
$$g_j = \sigma(V_j W_g). \quad (9)$$
  
654

655 where  $\sigma(\cdot)$  denotes the Sigmoid function.  
656657 **VGA output:**  
658

659 
$$z_i = \sum_{j=1}^n \alpha_{ij} (g_j V_j). \quad (10)$$
  
660

661 **Step 1: Base gradient expression.** The gradient of the loss  $L$  w.r.t.  $V_j$  is:  
662

663 
$$\frac{\partial L}{\partial V_j} = \sum_{i=1}^n \alpha_{ij} \frac{\partial(g_j V_j)}{\partial V_j} \frac{\partial L}{\partial z_i}. \quad (11)$$
  
664

665 **Step 2: Product rule for  $(g_j V_j)$ .** Since  $g_j$  depends on  $V_j$ :  
666

667 
$$\frac{\partial(g_j V_j)}{\partial V_j} = g_j I + \left( \frac{\partial g_j}{\partial V_j} \right)^T V_j, \quad (12)$$
  
668

669 this derivative is written in denominator layout convention,  $I \in \mathbb{R}^{d \times d}$  is the identity matrix.  
670671 **Step 3: Gate derivative.** Let  $u_j = V_j W_g$  (scalar). We have:  
672

673 
$$\frac{\partial u_j}{\partial V_j} = W_g^T, \quad \sigma'(u_j) = g_j(1 - g_j).$$
  
674

675 Therefore:  
676

677 
$$\frac{\partial g_j}{\partial V_j} = g_j(1 - g_j) W_g^T \quad (\in \mathbb{R}^{1 \times d}). \quad (13)$$
  
678

679 **Step 4: Full Jacobian of gated value.** Combining Equation (12) and Equation (13):  
680

681 
$$\frac{\partial(g_j V_j)}{\partial V_j} = g_j I + g_j(1 - g_j) W_g V_j, \quad (14)$$
  
682

683 yielding a  $d \times d$  matrix.  
684685 **Step 5: Final gradient.** Substituting Equation (14) into Equation (11):  
686

687 
$$\boxed{\frac{\partial L}{\partial V_j} = \sum_{i=1}^n \alpha_{ij} [g_j I + g_j(1 - g_j) W_g V_j] \frac{\partial L}{\partial z_i}} \quad (15)$$
  
688

689 **Interpretation.** The two terms inside the brackets correspond to two independent gradient pathways:  
690691 

- *Content Path:*  $g_j I$  — gradient through the semantic content of  $V_j$ , scaled by  $g_j$ .
- *Self-regulatory Path:*  $g_j(1 - g_j) W_g V_j$  — gradient arising from  $V_j$  influencing its own gate.

  
692693 If a sink token  $s$  has  $\alpha_{is} \rightarrow 1$  but  $g_s \rightarrow 0$ , both terms vanish:  
694

695 
$$g_s I \rightarrow 0, \quad g_s(1 - g_s) \rightarrow 0,$$
  
696

697 cleanly severing the gradient to  $V_s$  and breaking the mutual reinforcement cycle.  
698

## 702 B ARCHITECTURE DETAILS

704 This section provides a formal and detailed formulation of the Value-State Gated Attention (VGA)  
 705 mechanism. VGA modifies the standard attention by introducing a gate that modulates the final  
 706 output of the attention head. This gate, denoted as  $g$ , is computed directly from the value state  $V$ ,  
 707 creating a reactive feedback loop.

708 The core of the VGA mechanism is the computation of a dedicated gate for each attention head. In a  
 709 multi-head attention setting with  $h$  heads and a model dimension of  $d$ , the gate matrix  $g$  is computed  
 710 for all heads simultaneously from the complete value projection matrix  $V \in \mathbb{R}^{N \times d}$ . The gate matrix  
 711  $g \in \mathbb{R}^{N \times h}$  is computed as:

$$712 \quad 713 \quad g = \sigma(VW_g) \quad (16)$$

714 where  $W_g \in \mathbb{R}^{d \times h}$  is a single learnable weight matrix, and  $\sigma(\cdot)$  is the sigmoid function. Each column  
 715  $g_j$  in the resulting matrix  $g$  serves as the specific gate for the  $j$ -th attention head. The final output for  
 716 an individual head  $j$ , denoted  $O_{\text{VGA},j}$ , is then obtained by an element-wise product between its gate  
 717  $g_j$  and its standard attention output  $O_j$ :

$$718 \quad 719 \quad O_{\text{VGA},j} = g_j \odot O_j, \text{ where } O_j = \text{Attention}(Q_j, K_j, V_j). \quad (17)$$

720 For this multiplication, the gate vector  $g_j \in \mathbb{R}^{N \times 1}$  is broadcast across the feature dimension of  
 721 the head’s output  $O_j \in \mathbb{R}^{N \times d_{\text{head}}}$ , where  $d_{\text{head}} = d/h$ . This allows each head to have its output  
 722 modulated independently based on the same shared value-state representation. The final layer output  
 723 is formed by concatenating the gated head outputs, *i.e.*,  $\text{Concat}(O_{\text{VGA},1}, \dots, O_{\text{VGA},h})$ , followed by  
 724 the usual final linear projection.

725 This design ensures that VGA is a lightweight and minimally invasive module. It introduces only  
 726 a small number of new parameters  $W_g$  per attention head and, crucially, remains orthogonal to the  
 727 attention score computation. The original attention weights are calculated as usual, preserving the  
 728 mechanism’s ability to model long-range dependencies, while the gate provides a separate, reactive  
 729 pathway to control the informational output based on the value state.

## 731 C USING VGA FOR FINE-TUNING PRE-TRAINED MODELS

734 Table 3: VGA Retrofitting Analysis on Pre-trained GPT-2. Comparison of a vanilla pre-trained model  
 735 against a VGA equipped pre-trained model, both with 600K iterations, and two fine-tuning strategies  
 736 with 6K iterations. **Key Finding:** Fine-tuning with VGA, consuming only  $\sim 1\%$  of the pretraining  
 737 computation, significantly rectifies the pathology to a state comparable to scratch pre-training.

738 Model	739 Method	740 Perplexity ( $\downarrow$ )	741 Max I+O Norm ( $\downarrow$ )	742 Avg. kurtosis ( $\downarrow$ )
739 GPT-2	Vanilla	$17.03 \pm 0.00$	$256.84 \pm 18.77$	$13412.71 \pm 3.528.30$
	VGA	<b><math>16.52 \pm 0.01</math></b>	<b><math>12.37 \pm 1.28</math></b>	<b><math>31.27 \pm 6.71</math></b>
	Fine-tuning w/o VGA	$17.01 \pm 0.01$	$398.67 \pm 43.88$	$9863.87 \pm 2575.90$
	Fine-tuning w VGA	$16.94 \pm 0.01$	$24.05 \pm 4.73$	$32.47 \pm 2.95$

743 We investigated whether VGA could not only prevent extreme-token phenomena but also rectify them  
 744 in an existing, pathologically-developed model—a concept known as retrofitting.

745 We performed a short fine-tuning run (6,000 steps) of a GPT-2 model on the data that was used in  
 746 pre-training, comparing four variants: a vanilla pre-trained model, a VGA equipped pre-trained model,  
 747 the model fine-tuned without modification (Baseline) and the model fine-tuned after retrofitting the  
 748 VGA module (Retrofit).

749 The results in Table 3 decisively confirm VGA’s retrospective correction capability. Standard fine-  
 750 tuning (w/o VGA) failed to correct the pathology; in fact, the Max I+O Norm dramatically **worsened**  
 751 from 256.84 to 398.67, confirming the self-amplifying nature of the optimization pathology when  
 752 the VGA gate is absent. In stark contrast, retrofitting the VGA module immediately stabilized  
 753 the model: Max I+O Norm plummeted from 256.84 to **24.05** and Kurtosis dropped to **32.47**.  
 754 This strong regularization yielded the best Perplexity in the fine-tuning group (**16.94**). Crucially,  
 755 these stabilization metrics effectively approach to those achieved by pre-training VGA from scratch,  
 756 proving that VGA is highly effective even when introduced late in the learning process, significantly  
 757 expanding its practical utility.

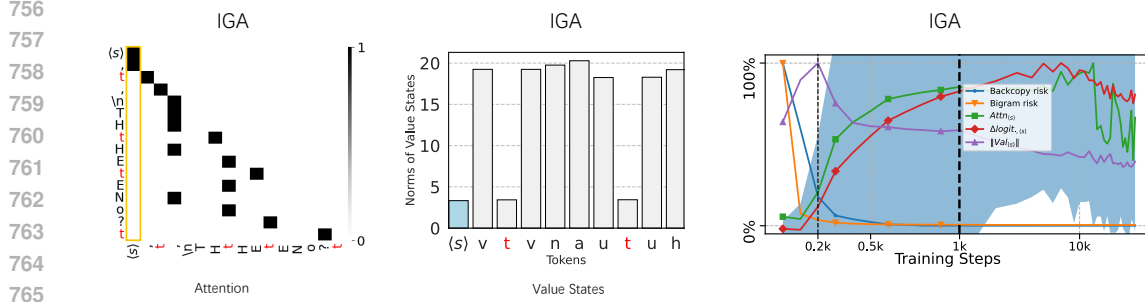


Figure 6: Analysis of IGA model on the Bigram-Backcopy task, left: Attention patterns, middle: Value status, right: Training dynamics.

#### D ANALYSIS OF IGA MODEL ON THE BIGRAM-BACKCOPY TASK

As shown in Figure 6, IGA mechanism reveals a mitigation of the pathological dynamics observed in the Vanilla model, though its performance remains inferior to VGA.

In terms of Attention Sinks, while the Vanilla model exhibits a quintessential pathological collapse, where non-trigger query attention concentrates severely onto the  $\langle s \rangle$  token (high  $Attn_{\langle s \rangle}$ ), the IGA model successfully dampens this effect. IGA achieves a more distributed attention pattern than Vanilla, yet it does not eliminate the pathological concentration as comprehensively as VGA, which maintains  $Attn_{\langle s \rangle}$  at healthy, non-extreme levels.

This partial alleviation directly translates into the Value-State Drains. The severe degradation of the start token's value-state norm,  $\|Val_{\langle s \rangle}\| \rightarrow 0$ , which characterizes the Vanilla model, is mitigated in IGA, preventing an aggressive reduction towards zero. However, the  $\|Val_{\langle s \rangle}\|$  in IGA does not stabilize at the maintained, non-pathological level achieved by the VGA model.

The distinct behavior is most clearly demonstrated in the Training Dynamics. The IGA model effectively slows and reduces the magnitude of the increase in the attention-related metrics ( $\|Val_{\langle s \rangle}\|$  and  $Attn_{\langle s \rangle}$ ), indicating a weaker pre-softmax bias and a less destructive feedback cycle compared to Vanilla. Nevertheless, the VGA model stands out by demonstrating fundamentally different training dynamics, where all pathological signals ( $\Delta logit_{\langle s \rangle}$ ,  $Attn_{\langle s \rangle}$  and  $\|Val_{\langle s \rangle}\|$ ) remain stable throughout training, confirming that VGA is the most effective mechanism for breaking the mutual reinforcement cycle.

#### E STATEMENT ON THE USE OF LLMs

During the preparation of this manuscript, we utilized large language models (LLMs) to assist with language editing and refinement. The purpose was to improve clarity, grammar, and overall readability. All scientific contributions, methodologies, and analyses are the original work of the authors, who take full responsibility for the content of this paper.